ELECTROCHEMISTRY

Closed-loop cathode recycling in solid-state batteries enabled by supramolecular electrolytes

Jiwoong Bae[1]†, Zhuoying Zhu[2], Jiajun Yan[3]‡, Dong-Min Kim[1,4], Youngmin Ko[1], Anubhav Jain[2], Brett A. Helms[1,3]*

Deconstructing solid-state batteries (SSBs) to physically separated cathode and solid-electrolyte particles remains intensive, as does the remanufacturing of cathodes and separators from the recovered materials. To address this challenge, we designed supramolecular organo-ionic (ORION) electrolytes that are viscoelastic solids at battery operating temperatures (−40° to 45°C) yet are viscoelastic liquids above 100°C, which enables both the fabrication of high-quality SSBs and the recycling of their cathodes at end of life. SSBs implementing ORION electrolytes alongside Li metal anodes and either LFP or NMC cathodes were operated for hundreds of cycles at 45°C with less than 20% capacity fade. Using a low-temperature solvent process, we isolated the cathode from the electrolyte and demonstrated that refurbished cells recover 90% of their initial capacity and sustain it for an additional 100 cycles with 84% capacity retention in their second life.

INTRODUCTION

Solid-state batteries (SSBs) are highly sought after to improve the safety of electric vehicles (*1*, *2*). However, the manufacturing of SSBs remains a challenge due to the difficulty in creating conformal interfaces between solid electrolyte particles and active materials in battery electrodes (*3*, *4*). Current interfacing strategies implement high temperature and high pressure to create composite electrodes from solid electrolytes and active materials and to assemble batteries comprising them alongside solid-electrolyte separators, metal anodes, and current collectors. In doing so, SSBs become difficult to recycle at end of life, owing to the adhesive character of interphases formed during thermal processing (*5*–*8*). Solid electrolytes whose properties facilitate SSB manufacturing, as well as deconstruction and recycling, at end of life, while offering sustainable SSB performance in the use phase, are urgently needed (*9*).

Here, we show that a tetrafunctional zwitterionic supramolecular building unit (SBU), 3,3′,3″,3‴-(1,3,5,7-tetraazaadamantane-1,3,5,7-tetraium-1,3,5,7-tetrayl)tetrakis(propane-1-sulfonate), networks both lithium salts and solvates thereof, creating from them organo-ionic (ORION) lithium-ion conductors (σ = 0.6 mS cm^{-1} at 45°C; Fig. 1). Notably, these ORION conductors are viscoelastic solid electrolytes at typical SSB operating temperatures (−45° to 45°C) yet viscoelastic liquids at temperatures of only 100°C. In the liquidus state, ORION conductors have excellent wetting characteristics for both lithium metal anodes and porous cathodes comprising either lithium iron phosphate (LFP) or $LiNi_{0.5}Mn_{0.3}Co_{0.2}O_2$ (NMC532) active materials. Consequently, ORION SSBs can be fabricated with conformal interfaces to both electrodes using low-intensity thermal processing. The assembled ORION SSBs showed 82% capacity retention after 100 cycles at a rate up to C/2 (0.1 mA cm^{-2}) at a vehicle relevant operating temperature (45°C). We further demonstrate that ORION solid electrolytes can be recovered from SSBs at end of life using a solvent process, which also enabled direct cathode recycling. Second-life ORION SSBs recovered 90% of their initial capacity and were able to sustain it for an additional 100 cycles with 84% capacity retention.

Our findings showcase the intriguing vantage point provided by supramolecular chemistry when exploring the design space of ORION conductors to meet ongoing codesign challenges in SSBs related to manufacturing, performance, and recycling circularity at end of life. From our molecular dynamics (MD) simulations, we find that their coordination chemistry across length scales is distinctive from small molecule, polymeric, and even zwitterionic ionic liquids (*10*–*16*). ORION conductors feature both structural lithium ions essential for solidification alongside mobile lithium ions essential for conductivity. These characteristics are broadly tunable through choice of salts, stoichiometry, and SBUs. Our insights suggest immense potential in harnessing the unique coordination chemistry, network structure and dynamics, and ion solvation and transport in supramolecular ionic solids to advance safer and more sustainable SSBs.

RESULTS

Physicochemical properties of ORION conductors

To create supramolecular ORION conductors, we hypothesized that lithium salts could be architected into viscoelastic solids by introducing to them polyfunctional zwitterionic small molecules, which, through their high dielectric constant and reversible coordination to Li^+, should give a network with sufficient dynamic character to allow thermal processing of SSBs. We further reasoned that because the materials comprised only molecular species, we would retain the ability to recover them using solvent, facilitating battery recycling at end of life.

To test this hypothesis, we synthesized a tetrafunctional zwitterionic SBU via ring opening of propane sultone with

[1]The Molecular Foundry, Lawrence Berkeley National Laboratory, 1 Cyclotron Road, Berkeley, CA 94720, USA. [2]Energy Storage and Distributed Resources Division, Lawrence Berkeley National Laboratory, 1 Cyclotron Road, Berkeley, CA 94720, USA. [3]Materials Sciences Division, Lawrence Berkeley National Laboratory, 1 Cyclotron Road, Berkeley, CA 94720, USA. [4]Joint Center for Energy Storage Research, Lawrence Berkeley National Laboratory, 1 Cyclotron Road, Berkeley, CA 94720, USA.
*Corresponding author. Email: bahelms@lbl.gov
†Present address: Department of Mechanical Engineering, Hanyang University, Seoul 04763, Republic of Korea.
‡Present address: School of Physical Science and Technology, ShanghaiTech University, Shanghai 201210, China.

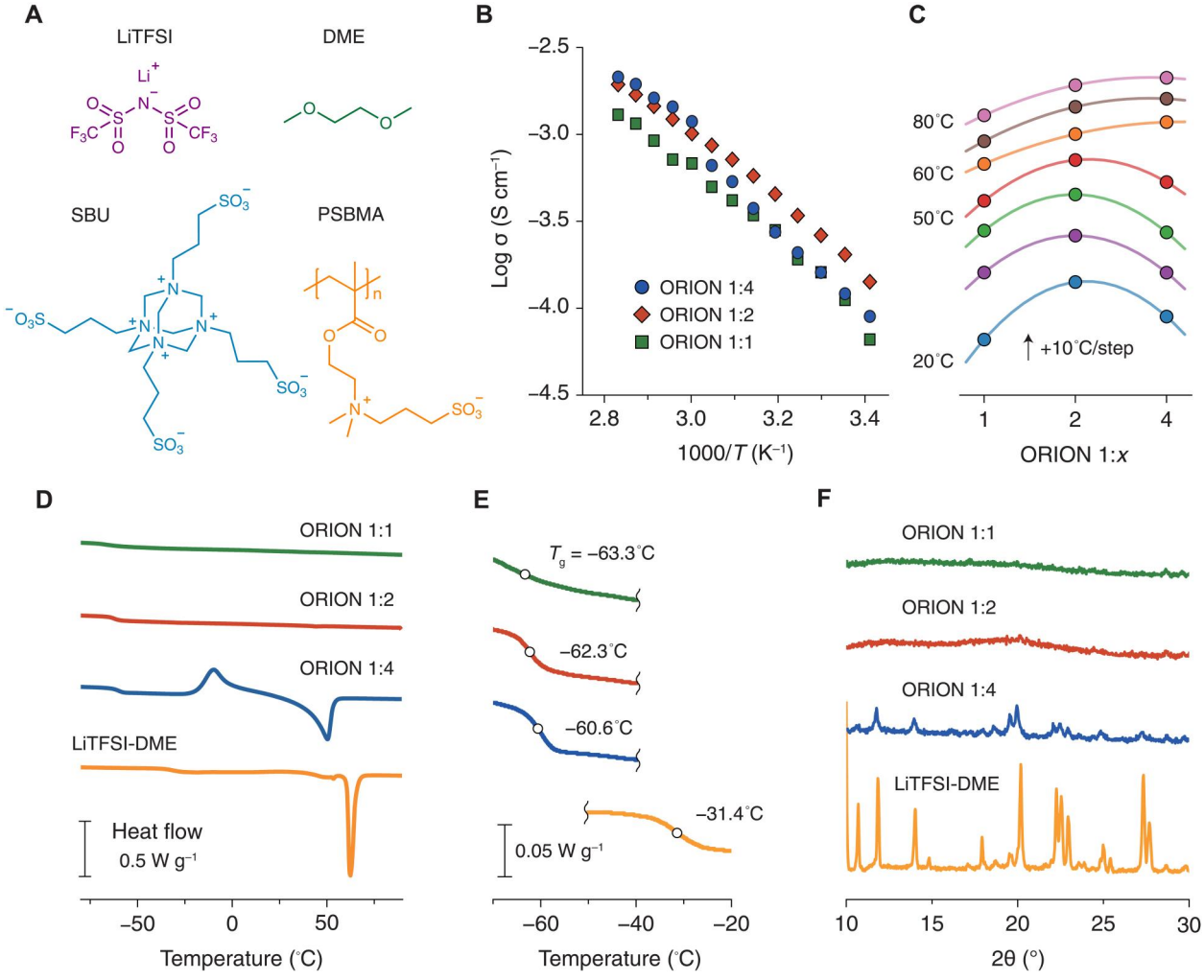

Fig. 1. Physicochemical properties of ORION conductors. (**A**) Supramolecular ORION conductors comprising lithium *bis*(trifluoromethanesulfonyl)imide (LiTFSI), 1,2-dimethoxyethane (DME), a tetrafunctional zwitterionic SBU, and a poly(sulfobetaine methacrylate) (PSBMA) viscosity modifier. (**B**) Temperature-dependent ionic conductivities (σ) for ORION conductors featuring an equimolar ratio of LiTFSI and DME and varying molar ratios of SO_3^-:Li^+ of 1:*x*, where *x* = 1, 2, or 4 and (**C**) comparison based on the molar ratio. (**D**) Differential scanning calorimetry (DSC) of ORION conductors and (**E**) identification of their glass transition temperatures (T_g). (**F**) Powder x-ray diffraction (PXRD) patterns for ORION conductors and a Li(DME)TFSI solvate crystalline solid.

hexamethylenetetramine (*17*). We ball-milled this SBU with various lithium salts, such as lithium *bis*(trifluoromethanesulfonyl)imide (LiTFSI), noting that across a range of molar ratios of SO_3^-:Li^+, the materials generated were glassy, brittle, and difficult to process thermally, consistent with highly networked material, but undesirable network dynamics. To decrease the Li^+ coordination number likely responsible for this behavior, we replaced LiTFSI with Li(DME)TFSI, i.e., its crystalline solvate with 1,2-dimethoxyethane (DME) (*18*). At molar ratios of SO_3^-:Li^+ of 1:*x*, where *x* = 1 to 4, we obtained malleable solids with excellent processability at remarkably low temperatures, typically below 100°C. For *x* exceeding 4, we obtained brittle solids because of an overabundance of Li(DME)TFSI crystals and phase separation. To manipulate the viscosity of these materials in the liquidus state, we found poly(sulfobetaine methacrylate)s (PSBMA) useful, which we prepared using free radical polymerization (*19*). As a result, we obtained viscoelastic solid at the temperature of 45°C, where electrochemical performance was evaluated (fig. S1). Together, these initial observations during synthesis suggested notably complex behavior at the molecular scale translating to bulk materials properties.

To understand the implications of these behaviors on structure–transport properties of the materials, we prepared a series of ORION conductors varying in the ratio of SBU to Li(DME)TFSI, keeping the portion of PSBMA fixed at 5% (w/w) relative to the SBU (Fig. 1A); we considered SO_3^-:Li^+ ratios of 1:1, 1:2, and 1:4, as these produced thermally processable solid-ion conductors. We measured their ionic conductivities over a temperature range of *T* = 20° to 80°C (Fig. 1B) by using electrochemical impedance spectroscopy (EIS) for samples thermally annealed between blocking stainless steel electrodes. Overall, ORION 1:2 demonstrated the highest conductivity: for example, σ = 0.58 mS cm^{-1} for ORION 1:2 at 45°C, compared to 0.34 mS cm^{-1} for ORION 1:1 and 0.38 mS cm^{-1} for ORION 1:4. We observed an abrupt increase in ionic conductivity on heating ORION 1:4 from 50°C to 60°C, suggesting a possible

phase transition in the material (Fig. 1C). Nonetheless, ORION 1:2 demonstrated the highest conductivity over the temperature region of interest for SSBs (i.e., from 20° to 55°C), which is comparable or higher than reported polymer or zwitterionic solid electrolytes (*15*, *20*). When we only increased the LiTFSI ratios, inhomogeneous mixtures were observed with a substantial drop in terms of conductivity, suggesting that ORION 1:2 fully used solvation sites (fig. S2). The activation energy for ORION 1:2 was about 0.44 eV, which confirms that ion conduction is not from liquid LiTFSI–DME (0.24 eV; fig. S3).

To provide a deeper understanding of the thermal properties of ORION conductors from the perspective of their phase transitions, we carried out differential scanning calorimetry (DSC) over a temperature range of −80° to 90°C (Fig. 1, D and E). Li(DME)TFSI exhibits a melting point of ~62°C. For ORION conductors with 1:1 and 1:2 ratios of SO_3^-:Li^+, we see complete dissolution of the Li(DME)TFSI solvate crystal into the SBU, such that there are no longer observable melting transitions and instead only glass transitions of T_g = −63°C and −62°C, respectively. At the highest loading of Li(DME)TFSI in the ORION conductor, we evidenced a melting transition at 50°C, as well as cold crystallization behavior at −10°C; both characteristics are exclusive to ORION 1:4. This indicates that ORION 1:4 is overloaded with Li(DME)TFSI and that small crystallites with a lower-than-bulk melting temperature persist in the material. Accordingly, we interpret the increase in ionic conductivity above 50°C to the melting of these crystallites, which produces more mobile ionic charge carriers than were available at lower temperatures.

The emerging picture is that ORION conductors are able to network Li(DME)TFSI into viscoelastic solid-ion conductors, whose processability and conductivity benefit from improved network dynamics tied to DME and its role in modifying the Li^+ coordination chemistry. However, there is an upper bound above which Li(DME)TFSI can be incorporated without also incurring the formation of crystal-in-glass composites. This is further supported by the powder x-ray diffraction (PXRD; Fig. 1F). Whereas the crystallinity of Li(DME)TFSI completely subsides in ORION 1:1 and 1:2, it rises in ORION 1:4, concurrent with the amorphous phase. This behavior is apparently driven by strong interactions between Li^+ and SO_3^-, as seen in the amorphization of LiTFSI when the SBU is present and DME is absent (fig. S4).

Solid solvation of lithium ions in ORION conductors

To understand how lithium salts were distributed in ORION conductors, we carried out MD simulation for ORION 1:1, 1:2, and 1:4 materials (Fig. 2), extracting from the simulations′ representative coordination motifs depicting Li^+, DME, and SBU (Fig. 2, A to C), as well as spatial relationships among SBUs (Fig. 2, D to F). Notably, we found that in the condensed phase, sulfonate end groups of the SBU were more strongly coordinating to Li^+ than DME or $TFSI^-$, as evidenced in the changes in coordination number at different Li^+:SO_3^- ratios (Fig. 2G and fig. S5).

For ORION 1:1 materials, the SBU sulfonates are predominantly coordinated to 82% of the desolvated Li^+ ions (Fig. 2A). In addition, 45% of the desolvated Li^+ ions bridge neighboring SBUs, forming a dense supramolecular network (Fig. 2D). The percentage of desolvated Li^+ ions categorized by numbers of neighboring sulfonates are depicted in Fig. 2H and table S1. Free DME in ORION 1:1 material segregates to the tetraalkylammonium core of the SBU with short O—H bond distances (2.3 to 2.8 Å), suggesting that hydrogen bonding may dictate that behavior (fig. S6). Together, these simulations corroborate our earlier findings that zwitterionic SBUs provide an effective solid-solvation environment for Li(DME)TFSI in ORION 1:1 materials, promoting the formation of a highly networked brittle and glassy solid, evidenced by a high degree of networking of 89% (see fig. S7).

In ORION 1:2 materials, we likewise observed a supramolecular network, consisting of desolvated Li^+ ions bridging neighboring SBUs through coordination to their sulfonates (Fig. 2B). Compared to ORION 1:1 materials, ORION 1:2 materials exhibited a lower degree of networking (69% for ORION 1:2 versus 89% for ORION 1:1; Fig. 2E and fig. S7). Free DME also engaged in hydrogen bonding to the SBU, as was the case with ORION 1:1. Solid solvation and speciation of Li^+ in ORION 1:2 materials were notably more complex: For example, we observe network terminations, consisting of 44% of Li^+ bound to only one sulfonate, with the remaining coordination sites taken up by DME and $TFSI^-$; we also find that 37% of Li^+ is unbound from the sulfonates (Fig. 2H and table S1). These new species are likely responsible for the higher ionic conductivity, along with gains coming from lower network density. In the case of free $TFSI^-$, they also form hydrogen bonds with the core of the SBU and C—H bonds in the pendants, particularly those adjacent to the sulfonate and tetraalkylammonium core. Such interactions may stretch the sulfonate arms, contributing to the segmental movement, which is assumed to improve Li^+ ionic conduction. While DME prefers to be coordinated only with Li^+ ions and the core of the SBU, $TFSI^-$ exhibits unbiased interactions with all the molecules including Li^+ ions, playing a role as a mediator in the supramolecular system (fig. S8).

In stark contrast, for ORION 1:4 materials, SBUs interacting with Li^+ were largely isolated or exhibited only short-range clustering behavior (fig. S9 and table S2); there was little network formation (Fig. 2, C and F). The degree of networking was reduced to 41% (fig. S7), and 60% of Li^+ ions did not bond to any of the available sulfonates, while those that did (33%) formed as network terminations (Fig. 2H). Moreover, there were insufficient numbers of sulfonate groups to associate with all of the available Li(DME)TFSI: Most of the SBU sulfonates were already bounded with at least one Li^+ ion nearby (see table S3). What remained of Li(DME)TFSI, unassociated with the SBUs, also exhibited crystallinity but less than might otherwise be expected, suggesting that SBU suppressed crystallization of the solvate. These simulation results were consistent with our DSC and PXRD data (Fig. 1). The architectural features in ORION conductors create unique coordination environments for facilitating ion conduction pathways, processability, interface and interphase creation, and resilience to volume changes in all solid-state cells, which are discussed below in turn.

Ion transport in ORION solid electrolytes

Chemomechanical properties of solid-ion conductors dictate their behaviors as solid electrolytes in batteries and other electrochemical devices, particularly for devices featuring metal anodes undergoing reversible plating and stripping (*21*, *22*). As noted above, ORION conductors feature, to varying degrees, both structural and mobile Li^+, depending on the ratio of Li^+:SO_3^-. To understand how solid solvation and Li^+ speciation affects their transport properties, we determined the critical current density at 45°C in Li-Li symmetric cells assembled with ORION 1:1, 1:2, and 1:4 conductors as solid

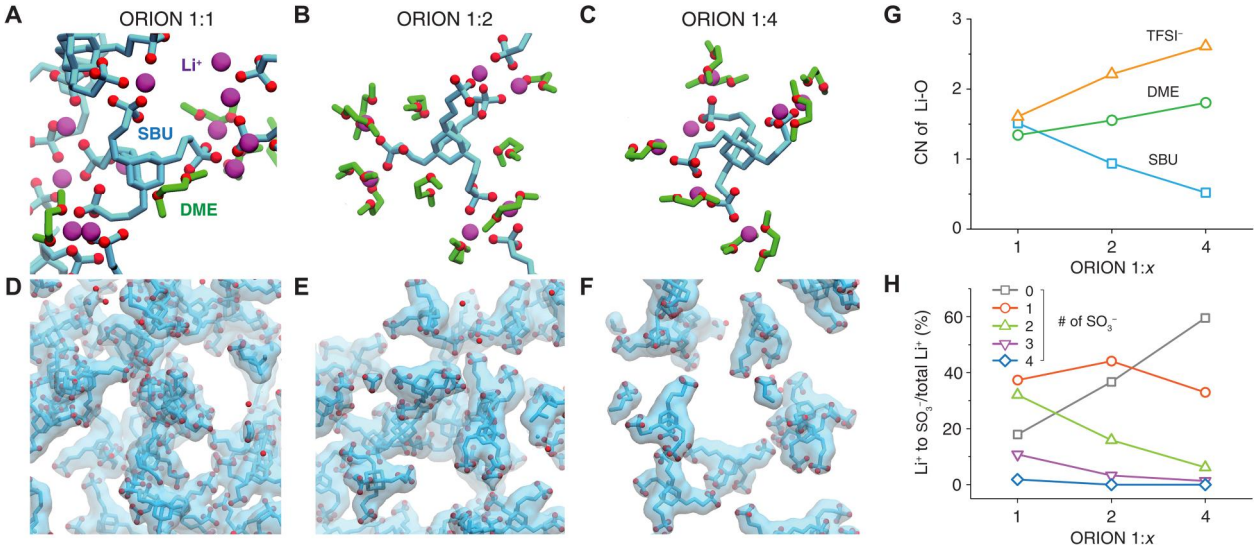

Fig. 2. MD simulations of ORION conductors. Snapshots of MD simulations of (**A**) ORION 1:1, (**B**) ORION 1:2, and (**C**) ORION 1:4, showing the interaction among SBU, Li^+, and DME ($TFSI^-$ has been removed for clarity). Blue molecules, SBU; purple spheres, Li^+; green molecules, DME; and small red spheres, oxygen atoms where Li^+ ions may coordinate. Simulated snapshots of SBU distributions in (**D**) ORION 1:1, (**E**) ORION 1:2, and (**F**) ORION 1:4. (**G**) Coordination number (CN) of Li^+ with O atoms in SBU, DME, and $TFSI^-$. PSBMA was not considered in the whole MD simulation for clarity. (**H**) The percentage of Li^+ ions that are coordinated with 0, 1, 2, 3, or 4 SO_3^- compared to the total number of Li^+ ions.

electrolytes (Fig. 3, A to C) (*23*). ORION 1:1 solid electrolytes exhibited the highest overpotentials by comparison to ORION 1:2 and 1:4 materials for lithium metal plating (and stripping) at a given current density. Divergences in overpotential with time, evidencing kinetic limitations, allowed us to quantify the critical current density of ORION 1:1 solid electrolytes as 0.30 mA cm^{-2} (Fig. 3A). For ORION 1:2, solid electrolytes, which showed the highest ionic conductivity (Fig. 1B), demonstrated improved Li^+ plating and stripping behaviors with lower overpotentials and a critical current density of 0.40 mA cm^{-2} (Fig. 3B). ORION 1:4 solid electrolytes, which are crystal-in-glass composites, initially evidenced large overpotentials for lithium plating/stripping and lastly soft short-circuiting, even at the lowest current density tested (0.10 mA cm^{-2}; Fig. 3C). The high performance of ORION 1:2 can be attributed to favorable solvation environments, especially majority of Li^+ ions bound to only one sulfonate, as well as the well-formed network, harnessing chemomechanical properties for both ion transport and mechanical integrity. These behaviors are intriguing

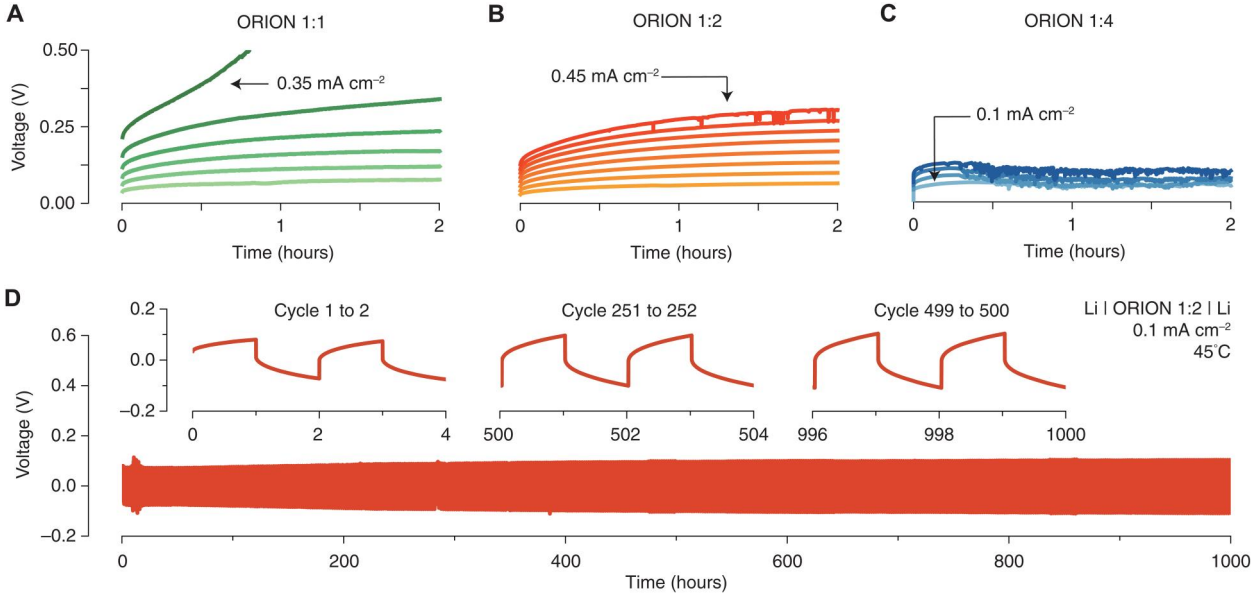

Fig. 3. Chemomechanical properties of ORION conductors in Li^+ plating and stripping. Critical current density measurements of (**A**) ORION 1:1, (**B**) ORION 1:2, and (**C**) ORION 1:4. (**D**) Long-term Li^+ plating/stripping cycling test with ORION 1:2 with the cycling range of 0 to 500 cycles. The inset shows three specific ranges of 1 to 2, 251 to 252, and 499 to 500 cycles. All electrochemical tests were conducted at 45°C in a Li–Li symmetric cell.

in that lithium coordination in these supramolecular solid electrolytes has profound effects on their structure–transport properties (*24*).

With the best-performing supramolecular solid electrolyte, ORION 1:2, we further investigated long-term cycling behavior for lithium plating and stripping in a Li–Li symmetric cell at 45°C (Fig. 3D). With a current density of 0.10 mA cm^{-2}, which is below the critical current density, ORION 1:2 solid electrolytes demonstrated stable cycling performance for 1000 hours (i.e., 500 cycles consisting of an alternating sequence of plating and stripping, each for a duration of 1 hour). The enlarged voltage profiles show that the overpotential slightly increased after 500 cycles, but the voltage plateaus are stable without divergence, where neither dendrites nor kinetic limitation was observed (Fig. 3D, inset). This suggested to us that the interphase generated between ORION 1:2 solid ion conductors and lithium metal was relatively stable over time (*25*–*27*). To provide evidence that this was the case, we carried out EIS of the symmetric cells over time at both 45° and 60°C, where the salient features were largely unchanged over a period of 10 hours (fig. S10).

Solid-state battery performance and closed-loop cathode recycling

Creating conformal interfaces in SSBs during battery assembly remains a challenge, owing to the hardness of constituent materials (*28*–*31*). We hypothesized that viscoelastic ion conductors, particularly those with a low-temperature transition between solid and liquidus states could maximize the interfacial area between the electrode and electrolyte materials. This would require that the supramolecular ORION solid electrolyte favorably wet the anode, cathode, and separator. To test this hypothesis, we melt-infiltrated conventional slurry-coated cathodes with the ORION 1:2 solid electrolyte by introducing ball-milled ORION 1:2 solid powders (Fig. 4A) to all-solid-state lithium metal cells, raising the temperature of the cell to 100°C for 5 min (Fig. 4B and fig. S11) and allowing the cell to cool to ambient temperature to solidify the electrolyte (Fig. 4C). We carried out synchrotron hard x-ray tomography in cells as assembled and after thermal annealing to characterize changes and the extent of interfacial coherence at lithium metal and within the pores of the cathode and separator [here, a woven mesh comprising polyethylene terephthalate (PET); Fig. 4, D and E] (*32*–*34*).

As assembled, the ball-milled ORION 1:2 solid electrolyte (which has not yet been thermally annealed) showed a dispersion of Li(DME)TFSI crystallites that manifest in the tomogram with highly contrasting features (Fig. 4D). The interface between Li metal and ball-milled ORION 1:2 materials was also rough (Fig. 4D, enlarged region). After 5 min at 100°C, Li(DME)TFSI crystallites were completely dissolved into the matrix comprising the zwitterionic SBU and polymeric viscosity modifier (Fig. 4E). The in situ formation of ORION 1:2 solid electrolyte and its infiltration into the separator and cathode produced a conformal interface at lithium metal (Fig. 4E, enlarged region) and the separator, whose weave we observed in cross section with no apparent aberrations in the interface with ORION 1:2 solid electrolytes. We further surmised the extent of cathode infiltration from the evolution in contrast from dark (empty pores) to light (ORION-filled pores) in that region of the tomogram and throughout the porous cathode from that perspective. This suggested to us that all solid-state ORION-infiltrated lithium metal cells should exhibit reversible cycling behavior, as all active materials necessary for cell cycling were in contact with the solid electrolyte after thermal annealing.

To understand how establishing conformal interfaces affects all-solid SSB performance with ORION 1:2 materials in place, we cycled Li|ORION|LFP cells at a current density of either 50 μA cm^{-2} (Fig. 5, A and B) or 100 μA cm^{-2} (Fig. 5, C and D), which

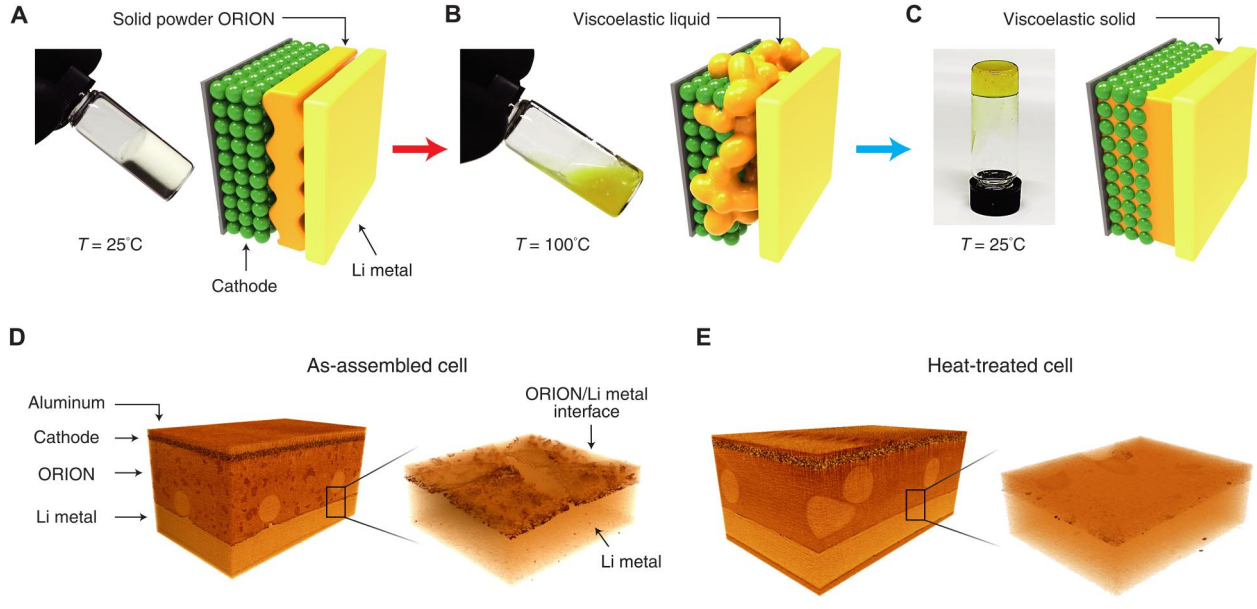

Fig. 4. Fabrication of solid-state cells with ORION conductors. (**A**) Fabricating all solid-state lithium metal cells from ball-milled ORION powders, which are initially sandwiched between a porous cathode and Li metal anode. (**B**) At and above 100°C, ORION conductors are viscoelastic liquids that infiltrate porous cathodes while also conforming to the Li metal surface. (**C**) After cooling, the ORION conductor solidifies, creating an all-solid-state lithium metal cell. Synchrotron hard x-ray tomography images of (**D**) an as-assembled ORION SSB and (**E**) an ORION SSB after thermal conditioning.

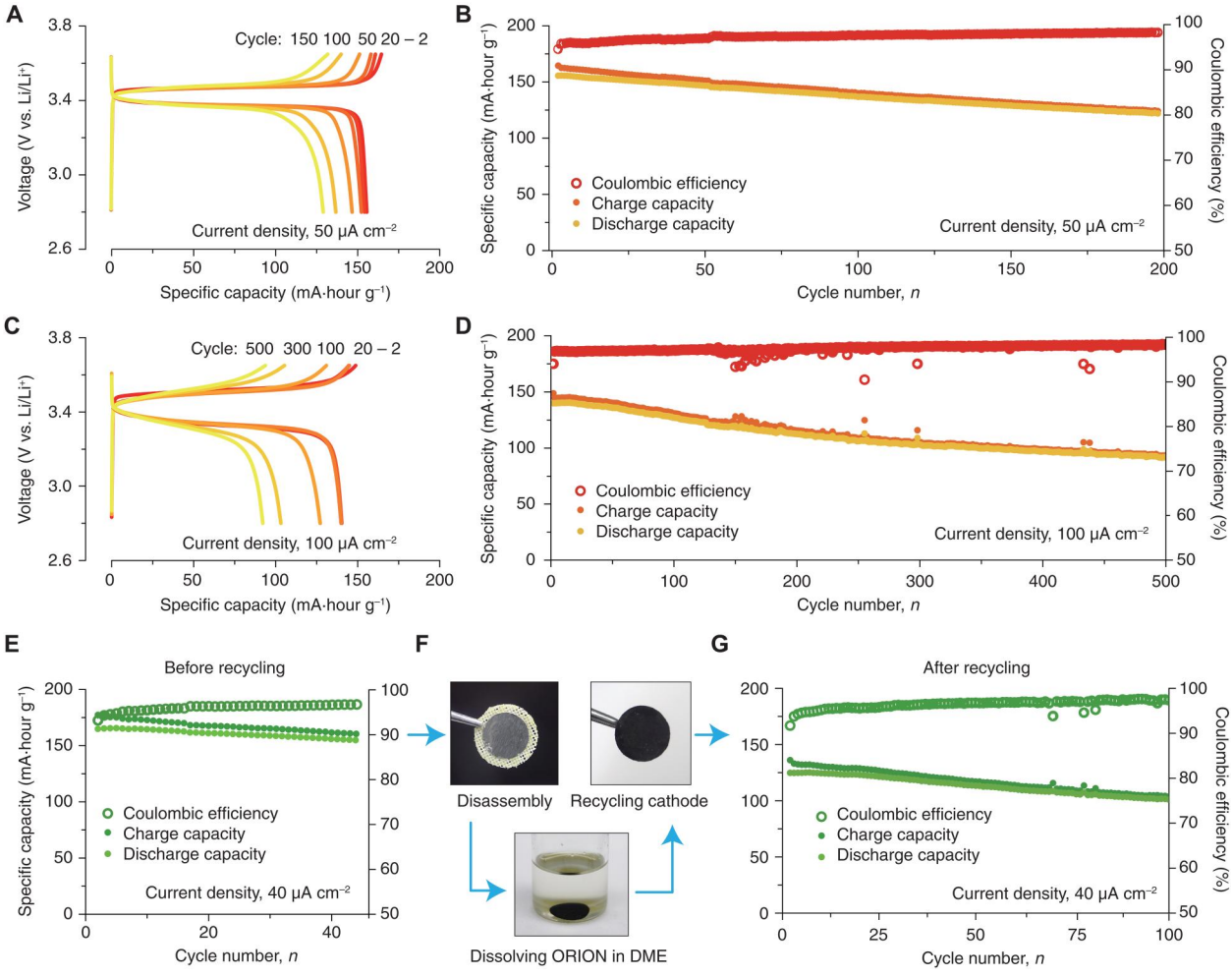

Fig. 5. Cell performance and closed-loop cathode recycling. (**A** and **C**) Voltage profiles and (**B** and **D**) cycling performances of Li|ORION|$LiFePO_4$ batteries under (A and B) 50 μA cm^{-2} and (C and D) 100 μA cm^{-2}. (**E** to **G**) Closed-loop direct cathode recycling. (E) Cycling performance of Li|ORION|$LiFePO_4$ battery before recycling, (F) cathode recycling process, and (G) cycling performance with recycled cathode. All electrochemical cell tests were conducted at 45°C.

are ~0.25 C and 0.5 C (1 C = 150 mA g^{-1}), respectively. Both cells achieved a specific capacity close to the theoretical capacity of LFP. Cells cycled at a current density of 50 μA cm^{-2} retained 85% capacity after 100 cycles, while those cycled at 100 μA cm^{-2} retained 82% capacity over the same period. Coulombic efficiency in both cases was higher than 98%. We also tested the voltage stability window of ORION 1:2 ion conductors and the cycling performance in Li|ORION|LiNMC532 all-solid-state cells at reversibly cycled at a current density of 200 μA cm^{-2}, where after 500 cycles, the cells retained a Coulombic efficiency higher than 99% after 500 cycles (figs. S12 and S13); we observed no shorting behavior. Together, these data indicate that ORION conductors are versatile in their ability to exploit a low-temperature solid–liquid phase transformation and favorable wetting characteristics to fabricate all-solid-state lithium metal cells that are rechargeable for hundreds of cycles. Owing to the remarkably slow area-specific impedance rise over time (fig. S14), we that reasoned it might be also feasible to deconstruct the all-solid-state cells, taking advantage of the solubility of ORION conductors, and close the loop in direct cathode recycling.

To demonstrate direct cathode recycling potential with Li|ORION|LFP (Fig. 5, E to G), we cycled it at a current density of 40 μA cm^{-2} until the capacity retention was ~90% of the initial capacity (Fig. 5E). We then disassembled the cell and immersed the LFP cathode in DME to dissolve the supramolecular solid ion conductor (Fig. 5f). We reassembled this cathode into a recycled Li|ORION|LFP cell and again subjected it to reversible cycling at 40 μA cm^{-2} (Fig. 5G). The recycled ORION cell showed initial capacity of ~90% compared to the capacity before direct cathode recycling. The slightly lower capacity is likely attributed to changes in mechanical integrity of the composite cathode, which may occur during disassembly. Notably, the recycled LFP cathode demonstrated 84% capacity retention after 100 cycles compared to the capacity of the second cycle of refurbished cell (assuming the first cycle was a formation cycle). The capacity fade rate before recycling was −0.14% per cycle (cycles 2 to 43 in Fig. 5E) while −0.19% per cycle (cycles 2 to 100 in Fig. 5G) after recycling. Thus, direct cathode recycling achieved similar long-term performance to the fade rate, capacity retention, and underlying Coulombic efficiency of a pristine LFP cathode [85% capacity retention from Fig. 5 (A and B)].

DISCUSSION

As the battery community contemplates the long-term prospects for achieving safe and stable operation of large vehicular powertrains for heavy transport, the elevation of SSB chemistries is at the forefront of discussion as is their underlying potential for resource recovery through chemical recycling (*35*–*39*). Whereas circularity and direct cathode recycling has been challenging to achieve with all-inorganic SSBs, we see exciting prospects for soft solid-ion conductors to meet codesign criteria across manufacturing and the use phase and at end of life. Moreover, revealing the underpinnings of these opportunities from fundamental supramolecular principles linking their structure–transport–processing–performance–recycling characteristics suggests rich areas of intrigue to explore long into the future.

MATERIALS AND METHODS

Preparation of ORION conductors

ORION powder was prepared in an argon glove box. SBU, LiTFSI, and DME were mixed with a ratio of SO_3^-:Li^+:DME = 1:1:1, 1:2:2, and 1:4:4 for ORION 1:1, ORION 1:2, and ORION 1:4, respectively. PSBMA was then added to the mixture with an amount with respect to the 5 weight % of SBU. All of the mixture was ground by mortar, which turns the mixture into a yellowish paste. After aging for 2 days in a glass vial in an argon glove box, the mixture solidified. The solid powder was ground by mortar again, and a fine white powder of ORION can be obtained finally.

Materials characterization

DSC was performed using TA Instrument DSC 2500. A set of T-zero hermetic pan and the T-zero press was first transferred into a glove box filled with argon. The pan was tared, and an aliquot of the sample was weighed inside the pan. Then, the pan was pressed and transferred to the autosampler of the instrument, which was equilibrated at −90°C. After 5 min of isotherm, the temperature was ramped at 10°C min^{-1} to 90°C and held for an additional 5 min before ramping back to −90°C. The same cycle was repeated five times. The second cycle was reported when no apparent difference was seen in cycles 2 to 6. XRD was conducted using a Rigaku MiniFlex 6G x-ray diffractometer, operated with a Cu Kα radiation with 600 W of x-ray source at 40 kV and 15 mA. To avoid exposure of ORION to ambient air, particularly moisture, the XRD samples were prepared in an argon glove box, where 10 to 20 mg of ORION was sealed in an air-tight holder with a beryllium window. ^{1}H nuclear magnetic resonance (NMR) was performed using a Bruker Avance 500 NMR spectrometer. Deuterium oxide was used as the solvent.

Electrochemical characterization

Electrochemical studies were performed using CR2032 coin cells. The conductivity and EIS impedance were measured by BioLogic VMP3 in an environmental chamber for temperature control. Li symmetric cell test, Li|ORION|LFP and Li|ORION|NMC cell test were carried out in an oven at 45°C. For the critical current density test, Li symmetric cells were allowed to rest for 12 hours; then, three formation cycles of 0.10 mA cm^{-2} for 5 hours and rest for 2 hours were applied. The critical current density was measured with 2 hours of plating and 2 hours of rest starting from 0.10 mA cm^{-2} with intervals of 0.05 mA cm^{-2}. Li symmetric cycling performance was conducted under 0.10 mA cm^{-2} for 1 hour per step. For the linear sweep voltammetry test, Li|ORION|stainless steel cells were assembled in a coin cell. Then, voltage was swept from open circuit voltage to 5 V versus Li/Li^+ with a scan rate of 0.1 mV s^{-1}. LFP and NMC cathodes were prepared by slurry coating on an aluminum current collector with 8:1:1 ratio of active material:Super P:polyvinylidene fluoride in *N*-methyl-2-pyrrolidinone (NMP) solvent. The coated electrode was dried at 120°C in vacuum. The active material loading is 1.0 to 1.2 mg cm^{-2}. For the cycling performance, the Li|ORION|LFP cell was tested under a current density of either 0.05 or 0.1 mA cm^{-2}, while 0.04 mA cm^{-2} was used for the recycling test. The Li|ORION|NMC cell used a current density of 0.2 mA cm^{-2}. For all the cell tests, ORION powder was pressed with a PET mesh that turns into a pellet of ORION. The PET mesh is about 0.3 mm with 50% porosity.

Synchrotron hard x-ray microtomography

Li|ORION|NMC cells were assembled and sealed in Al-laminated pouches in an argon glove box. For the heat-treated cell, a pouch was heat-treated in a vacuum oven at 100°C overnight. Monochromatic hard x-ray (23 keV) microtomography was then carried out on beamline 8.3.2 at the Advanced Light Source at Lawrence Berkeley National Laboratory. The samples were rotated 180° under the x-ray, and the shadows cast by the samples were converted to image stacks with ~1104 images in each stack. The stacks were resliced with ImageJ software to obtain an aligned image stack. Dragonfly software was used to display three dimensionally from the image stack.

Supplementary Materials

This PDF file includes:

Figs. S1 to S14
Tables S1 to S3
References

REFERENCES AND NOTES

1. Q. Zhao, S. Stalin, C. Z. Zhao, L. A. Archer, Designing solid-state electrolytes for safe, energy-dense batteries. *Nat. Rev. Mater.* **5**, 229–252 (2020).
2. J. Janek, W. G. Zeier, Challenges in speeding up solid-state battery development. *Nat. Energy* **8**, 230–240 (2023).
3. J. Lee, T. Lee, K. Char, K. J. Kim, J. W. Choi, Issues and advances in scaling up sulfide-based all-solid-state batteries. *Acc. Chem. Res.* **54**, 3390–3402 (2021).
4. K. J. Huang, G. Ceder, E. A. Olivetti, Manufacturing scalability implications of materials choice in inorganic solid-state batteries. *Joule* **5**, 564–580 (2021).
5. D. H. S. Tan, A. Banerjee, Z. Chen, Y. S. Meng, From nanoscale interface characterization to sustainable energy storage using all-solid-state batteries. *Nat. Nanotechnol.* **15**, 170–180 (2020).
6. L. Azhari, S. Bong, X. T. Ma, Y. Wang, Recycling for all solid-state lithium-ion batteries. *Matter* **3**, 1845–1861 (2020).
7. M. Chen, X. Ma, B. Chen, R. Arsenault, P. Karlson, N. Simon, Y. Wang, Recycling end-of-life electric vehicle lithium-ion batteries. *Joule* **3**, 2622–2646 (2019).
8. E. Fan, L. Li, Z. Wang, J. Lin, Y. Huang, Y. Yao, R. Chen, F. Wu, Sustainable recycling technology for Li-ion batteries and beyond: Challenges and future prospects. *Chem. Rev.* **120**, 7020–7063 (2020).
9. Q. Zhao, X. Liu, S. Stalin, K. Khan, L. A. Archer, Solid-state polymer electrolytes with in-built fast interfacial transport for secondary lithium batteries. *Nat. Energy* **4**, 365–373 (2019).
10. K. Xu, Electrolytes and interphases in Li-ion batteries and beyond. *Chem. Rev.* **114**, 11503–11618 (2014).
11. Y. Yamada, J. H. Wang, S. Ko, E. Watanabe, A. Yamada, Advances and issues in developing salt-concentrated battery electrolytes. *Nat. Energy* **4**, 269–280 (2019).

12. M. J. Lee, J. Han, K. Lee, Y. J. Lee, B. G. Kim, K. N. Jung, B. J. Kim, S. W. Lee, Elastomeric electrolytes for high-energy solid-state lithium batteries. *Nature* **601**, 217–222 (2022).
13. F. F. Chen, X. E. Wang, M. Armand, M. Forsyth, Cationic polymer-in-salt electrolytes for fast metal ion conduction and solid-state battery applications. *Nat. Mater.* **21**, 1175–1182 (2022).
14. S. D. Jones, H. Nguyen, P. M. Richardson, Y. Q. Chen, K. E. Wyckoff, C. J. Hawker, R. J. Clément, G. H. Fredrickson, R. A. Segalman, Design of polymeric zwitterionic solid electrolytes with superionic lithium transport. *ACS. Central. Sci.* **8**, 169–175 (2022).
15. F. Makhlooghiazad, L. A. O'Dell, L. Porcarelli, C. Forsyth, N. Quazi, M. Asadi, O. Hutt, D. Mecerreyes, M. Forsyth, J. M. Pringle, Zwitterionic materials with disorder and plasticity and their application as non-volatile solid or liquid electrolytes. *Nat. Mater.* **21**, 228–236 (2022).
16. M. Armand, F. Endres, D. R. MacFarlane, H. Ohno, B. Scrosati, Ionic-liquid materials for the electrochemical challenges of the future. *Nat. Mater.* **8**, 621–629 (2009).
17. S. Safaei, I. Mohammadpoor-Baltork, A. R. Khosropour, M. Moghadam, S. Tangestaninejad, V. Mirkhani, R. Kia, Application of a multi-SO_3H Brønsted acidic ionic liquid in water: A highly efficient and reusable catalyst for the regioselective and scaled-up synthesis of pyrazoles under mild conditions. *RSC Adv.* **2**, 5610–5616 (2012).
18. D. Brouillette, D. E. Irish, N. J. Taylor, G. Perron, M. Odziemkowski, J. E. Desnoyers, Stable solvates in solution of lithium bis(trifluoromethylsulfone)imide in glymes and other aprotic solvents: Phase diagrams, crystallography and raman spectroscopy. *Phys. Chem. Chem. Phys.* **4**, 6063–6071 (2002).
19. V. Hildebrand, A. Laschewsky, M. Päch, P. Müller-Buschbaum, C. M. Papadakis, Effect of the zwitterion structure on the thermo-responsive behaviour of poly(sulfobetaine methacrylates). *Polym. Chem.* **8**, 310–322 (2017).
20. J. Bae, Y. Li, J. Zhang, X. Zhou, F. Zhao, Y. Shi, J. B. Goodenough, G. Yu, A 3D nanostructured hydrogel-framework-derived high-performance composite polymer lithium-ion electrolyte. *Angew. Chem. Int. Ed.* **57**, 2096–2100 (2018).
21. C. Y. Fu, V. Venturi, J. Kim, Z. Ahmad, A. W. Ells, V. Viswanathan, B. A. Helms, Universal chemomechanical design rules for solid-ion conductors to prevent dendrite formation in lithium metal batteries. *Nat. Mater.* **19**, 758–766 (2020).
22. Z. Ahmad, V. Viswanathan, Stability of electrodeposition at solid-solid interfaces and implications for metal anodes. *Phys. Rev. Lett.* **119**, 056003 (2017).
23. Y. Lu, C. Z. Zhao, H. Yuan, X. B. Cheng, J. Q. Huang, Q. Zhang, Critical current density in solid-state lithium metal batteries: Mechanism, influences, and strategies. *Adv. Funct. Mater.* **31**, 2009925 (2021).
24. J. Lopez, D. G. Mackanic, Y. Cui, Z. Bao, Designing polymers for advanced battery chemistries. *Nat. Rev. Mater.* **4**, 312–330 (2019).
25. F. Shi, A. Pei, D. T. Boyle, J. Xie, X. Yu, X. Zhang, Y. Cui, Lithium metal stripping beneath the solid electrolyte interphase. *Proc. Natl. Acad. Sci. U.S.A.* **115**, 8529–8534 (2018).
26. J. Liu, Z. Bao, Y. Cui, E. J. Dufek, J. B. Goodenough, P. Khalifah, Q. Li, B. Y. Liaw, P. Liu, A. Manthiram, Y. S. Meng, V. R. Subramanian, M. F. Toney, V. V. Viswanathan, M. S. Whittingham, J. Xiao, W. Xu, J. Yang, X. Q. Yang, J. G. Zhang, Pathways for practical high-energy long-cycling lithium metal batteries. *Nat. Energy* **4**, 180–186 (2019).
27. P. Albertus, S. Babinec, S. Litzelman, A. Newman, Status and challenges in enabling the lithium metal electrode for high-energy and low-cost rechargeable batteries. *Nat. Energy* **3**, 16–21 (2018).
28. R. Koerver, I. Aygün, T. Leichtweiß, C. Dietrich, W. Zhang, J. O. Binder, P. Hartmann, W. G. Zeier, J. Janek, Capacity fade in solid-state batteries: Interphase formation and chemomechanical processes in nickel-rich layered oxide cathodes and lithium thiophosphate solid electrolytes. *Chem. Mater.* **29**, 5574–5582 (2017).
29. Y. Xiao, K. Turcheniuk, A. Narla, A. Y. Song, X. Ren, A. Magasinski, A. Jain, S. Huang, H. Lee, G. Yushin, Electrolyte melt infiltration for scalable manufacturing of inorganic all-solid-state lithium-ion batteries. *Nat. Mater.* **20**, 984–990 (2021).
30. J. Lee, K. Lee, T. Lee, H. Kim, K. Kim, W. Cho, A. Coskun, K. Char, J. W. Choi, In situ deprotection of polymeric binders for solution-processible sulfide-based all-solid-state batteries. *Adv. Mater.* **32**, 2001702 (2020).
31. D. H. Kim, D. Y. Oh, K. H. Park, Y. E. Choi, Y. J. Nam, H. A. Lee, S. M. Lee, Y. S. Jung, Infiltration of solution-processable solid electrolytes into conventional Li-ion-battery electrodes for all-solid-state Li-ion batteries. *Nano Lett.* **17**, 3013–3020 (2017).
32. K. J. Harry, D. T. Hallinan, D. Y. Parkinson, A. A. MacDowell, N. P. Balsara, Detection of subsurface structures underneath dendrites formed on cycled lithium metal electrodes. *Nat. Mater.* **13**, 69–73 (2014).
33. M. J. Baran, M. E. Carrington, S. Sahu, A. Baskin, J. Song, M. A. Baird, K. S. Han, K. T. Mueller, S. J. Teat, S. M. Meckler, C. Fu, D. Prendergast, B. A. Helms, Diversity-oriented synthesis of polymer membranes with ion solvation cages. *Nature* **592**, 225–231 (2021).
34. V. Wood, X-ray tomography for battery research and development. *Nat. Rev. Mater.* **3**, 293–295 (2018).
35. W. L. Fredericks, S. Sripad, G. C. Bower, V. Viswanathan, Performance metrics required of next-generation batteries to electrify vertical takeoff and landing (VTOL) aircraft. *ACS Energy Lett.* **3**, 2989–2994 (2018).
36. V. Viswanathan, B. M. Knapp, Potential for electric aircraft. *Nat. Sustain.* **2**, 88–89 (2019).
37. S. Sripad, V. Viswanathan, Quantifying the economic case for electric semi-trucks. *ACS Energy Lett.* **4**, 149–155 (2019).
38. M. K. Tran, M. T. F. Rodrigues, K. Kato, G. Babu, P. M. Ajayan, Deep eutectic solvents for cathode recycling of Li-ion batteries. *Nat. Energy* **4**, 339–345 (2019).
39. Y. Wang, D. Lu, M. Bowden, P. Z. el Khoury, K. S. Han, Z. D. Deng, J. Xiao, J. G. Zhang, J. Liu, Mechanism of formation of $Li_7P_3S_{11}$ solid electrolytes through liquid phase synthesis. *Chem. Mater.* **30**, 990–997 (2018).
40. S. Plimpton, Fast parallel algorithms for short-range molecular dynamics. *J. Comput. Phys.* **117**, 1–19 (1995).
41. B. Doherty, X. Zhong, S. Gathiaka, B. Li, O. Acevedo, Revisiting OPLS force field parameters for ionic liquid simulations. *J. Chem. Theory Comput.* **13**, 6131–6145 (2017).
42. L. S. Dodda, I. Cabeza de Vaca, J. Tirado-Rives, W. L. Jorgensen, LigParGen web server: An automatic OPLS-AA parameter generator for organic ligands. *Nucleic Acids Res.* **45**, W331–W336 (2017).
43. L. S. Dodda, J. Z. Vilseck, J. Tirado-Rives, W. L. Jorgensen, 1.14*CM1A-LBCC: Localized bond-charge corrected CM1A charges for condensed-phase simulations. *J. Phys. Chem. B* **121**, 3864–3870 (2017).
44. W. L. Jorgensen, J. Tirado-Rives, Potential energy functions for atomic-level simulations of water and organic and biomolecular systems. *Proc. Natl. Acad. Sci. U.S.A.* **102**, 6665–6670 (2005).
45. J. N. Canongia Lopes, A. A. H. Pádua, Molecular force field for ionic liquids composed of triflate or bistriflylimide anions. *J. Phys. Chem. B* **108**, 16893–16898 (2004).
46. K. P. Jensen, W. L. Jorgensen, Halide, ammonium, and alkali metal ion parameters for modeling aqueous solutions. *J. Chem. Theory Comput.* **2**, 1499–1509 (2006).
47. K. P. Jensen, W. L. Jorgensen, *Computer Simulation Using Particles* (Adam Hilger, 1989).
48. L. Martínez, R. Andrade, E. G. Birgin, J. M. Martínez, PACKMOL: A package for building initial configurations for molecular dynamics simulations. *J. Comput. Chem.* **30**, 2157–2164 (2009).
49. N. Michaud-Agrawal, E. J. Denning, T. B. Woolf, O. Beckstein, MDAnalysis: A toolkit for the analysis of molecular dynamics simulations. *J. Comput. Chem.* **32**, 2319–2327 (2011).

Acknowledgments

Funding: The technical scope of this work was primarily supported by the Laboratory Directed Research and Development Program of Lawrence Berkeley National Laboratory under U.S. Department of Energy contract no. DE-AC02–05CH11231. Portions of this work, including chemical synthesis and characterization, were carried out as a user project at the Molecular Foundry, which is supported by the Office of Science, Office of Basic Energy Sciences of the U.S. Department of Energy under contract no. DE-AC02-05CH11231. Synchrotron hard x-ray microtomography was carried out at the Advanced Light Source, which is a U.S. Department of Energy Office of Science User Facility operated under the same contract. Computation was carried out at the National Energy Research Scientific Computing Center (NERSC), a U.S. Department of Energy Office of Science User Facility operated under the same contract. D.-M.K. acknowledges support from Joint Center for Energy Storage Research (JCESR), an Energy Innovation Hub funded by the U.S. Department of Energy, Office of Science, Office of Basic Energy Sciences. Y.K. acknowledges support from the Advanced Research Projects Agency-Energy (ARPA-E), U.S. Department of Energy, under award number DE-AR0001450. **Author contributions:** B.A.H. designed and directed the study. J.B. conducted sample preparation for analysis, electrochemical tests, and visualization of MD simulations. J.Y. synthesized ORION components and conducted NMR and DSC analysis. A.J. designed and directed the theoretical study. Z.Z. conducted MD simulations and analyzed the network architectures. D.-M.K. assisted with DSC and analysis. Y.K. conducted LFP full cell tests. B.A.H., J.B., and Z.Z. wrote the paper with contributions from all coauthors. **Competing interests:** J.B., J.Y., D.-M.K., and B.A.H. are inventors on U.S. provisional patent application 63/488,714 submitted by Lawrence Berkeley National Laboratory, which covers the ORION solid electrolytes and aspects of their use. B.A.H. has a financial interest in Sepion Technologies and Cyklos Materials, which are commercializing lithium metal batteries and circular plastics, respectively. The other authors declare that they have no other competing interests. **Data and materials availability:** All data needed to evaluate the conclusions in the paper are present in the paper and/or the Supplementary Materials.

Submitted 21 March 2023
Accepted 12 July 2023
Published 11 August 2023
10.1126/sciadv.adh9020

ScienceAdvances

Closed-loop cathode recycling in solid-state batteries enabled by supramolecular electrolytes

Jiwoong Bae, Zhuoying Zhu, Jiajun Yan, Dong-Min Kim, Youngmin Ko, Anubhav Jain, and Brett A. Helms

Sci. Adv., **9** (32), eadh9020.
DOI: 10.1126/sciadv.adh9020

Science Advances (ISSN) is published by the American Association for the Advancement of Science. 1200 New York Avenue NW, Washington, DC 20005. The title *Science Advances* is a registered trademark of AAAS.